

Magnetocaloric properties and critical behavior of $\text{Co}_2\text{Cr}_{1-x}\text{Mn}_x\text{Al}$ Heusler alloys

Priyanka Nehla,¹ V. K. Anand,^{2,3} Bastian Klemke,² Bella Lake,² and R. S. Dhaka^{1,*}

¹*Department of Physics, Indian Institute of Technology Delhi, Hauz Khas, New Delhi-110016, India*

²*Helmholtz-Zentrum Berlin für Materialien und Energie GmbH, Hahn-Meitner Platz 1, D-14109 Berlin, Germany*

³*Department of Physics, SRM University, AP - Amaravati, 522502, Andhra Pradesh, India*

(Dated: February 19, 2024)

We study the magnetocaloric effect and critical behavior of $\text{Co}_2\text{Cr}_{1-x}\text{Mn}_x\text{Al}$ ($x = 0.25, 0.5, 0.75$) Heusler alloys across the ferromagnetic (FM) transition (T_C). The Rietveld refinement of x-ray diffraction patterns exhibit single phase cubic structure for all the samples. The temperature dependent magnetic susceptibility $\chi(T)$ data show a systematic enhancement in the Curie temperature and effective magnetic moment with Mn concentration, which is consistent with the Slater-Pauling behavior. The $M(H)$ isotherms also exhibit the FM ordering and the analysis of $\chi(T)$ data indicates the nature of the phase transition to be a second order, which is further supported by scaling of the entropy curves and Arrott plot. Interestingly, the Mn substitution causes an increase in the magnetic entropy change and hence large relative cooling power for multi-stage magnetic refrigerator applications. In order to understand the nature of the magnetic phase transition we examine the critical exponents β , γ , δ for the $x = 0.75$ sample by the modified Arrott plot and the critical isotherm analysis, which is further confirmed by Kouvel-Fisher method and Widom scaling relation, respectively. The estimated values of $\beta = 0.507$, $\gamma = 1.056$, $\delta = 3.084$ are found to be close to the mean field theoretical values. The renormalized isotherms (m vs h) corresponding to these exponent values collapse into two branches, above and below T_C that validates our analysis. Our results suggest for the existence of long-range FM interactions, which decays slower than power law as $J(r) \sim r^{-4.5}$ for a 3 dimensional mean field theory.

INTRODUCTION

Heusler alloys have attracted great attention to the scientific community after the discovery of ferromagnetism in Cu_2MnSn alloy in 1903 [1]. The full Heusler alloys, having X_2YZ formula, crystallize in cubic structure with $Fm\bar{3}m$ space group, where X , Y are the transition elements, and Z is the main group element [2–4]. In recent years, many unique physical properties have been found in Heusler alloys such as shape memory effect [5–8], magnetoresistance (MR) [9], half metallicity, spin filters, and spin injection devices [10–12]. The half metallic ferromagnets belong to a new class of materials, in which the band structure shows semiconducting nature for one spin channel and metallic for other spin channel, and it was first observed in NiMnSb Heusler alloys by Groot *et al.* [11]. The observed high magnetic moment, the Curie temperature (T_C) well above the room temperature and half metallic ferromagnetic (HMF) nature in Heusler alloys (in particular Co-based) make them attractive candidate for spintronics applications [12–16]. In this direction, the ferromagnetic Co_2CrAl is particularly interesting because of its many useful physical properties; for example T_C (330 K) just above room temperature, theoretically predicted 100% spin polarization, anomalous Hall conductivity, and the calculated magnetic moment of $3\mu_B$ [17–19]. Intriguingly, the Co_2MnAl Heusler alloy has been also predicted to show half metallic ferromagnet with the T_C value much higher (about 665 K) and the total magnetic moment equal to $4\mu_B/\text{f.u.}$, which follow the Slater-Pauling behavior [20–22]. The appearance of Weyl points near the Fermi energy may cause the anoma-

lous Hall conductivity in these materials [23]. Therefore, it is vital to study the effect of Mn substitution at Cr site in Co_2CrAl to understand the magnetic properties, which play crucial role in practical applications [24, 25].

Apart from the HMF nature, magnetocaloric effect (MCE) is one of the most interesting properties found in Heusler alloys, which is useful in magnetic refrigerators [26]. The MCE is a phenomena where a material heats up or cools down on the application or removal of the magnetic field. Initially, rare earth materials were considered to be the best candidates for MCE because of their high value of magnetic entropy change (ΔS_m). For example, ferromagnetic element Gd which has a very high magnetic moment shows T_C around room temperature and $-\Delta S_m = 10 \text{ J/kg.K}$ at 5 Tesla field change [27]. However, the high cost of Gd makes it undesirable for the application of commercial magnetic refrigerator. As the Heusler alloys also have the potential for magnetic refrigerator applications, extensive efforts have been made on the study of magnetocaloric properties in these materials [28–30]. In particular Ni–Mn–Z ($Z = \text{In, Sn, Sb}$) shape memory Heusler alloys, which show first order phase transition (FOPT), have been widely explored for the magnetic refrigerator applications [31–33]. These alloys exhibit both conventional and inverse MCE i.e. negative and positive magnetic entropy change (ΔS_m), respectively. This remarkable feature of these shape memory alloys is because of the coexistence of both structural and magnetic transitions. These properties are strongly correlated to each other and can easily be tuned with sample composition [34–36]. Although, the peak value of ΔS_m is found to be very high in FOPT alloys

which is desirable for better cooling efficiency, but the presence of thermal and magnetic hysteresis limits their use in practical applications [37, 38].

In recent years, the magnetocaloric properties have been explored in Co-based Heusler alloys. These alloys show a second order phase transition (SOPT), and have advantages of broad operating temperature range [39] and absence of thermal and/or magnetic hysteresis [40, 41]. In order to better understand the magnetic transition in these alloys, the study of critical phenomena in the vicinity of the phase transition will have a great significance. The critical behavior across the paramagnetic to ferromagnetic (PM-FM) transition of perovskite manganites in double exchange model was first explained by long range mean-field theory. A few detailed studies of the critical phenomena in double exchange ferromagnetic $\text{La}_{1-x}\text{A}_x\text{MnO}_3$ ($\text{A} = \text{Sr}, \text{Ca}$) have been reported in literature [42–44]. Moreover, the analysis of critical exponents for appropriate model proves very informative in examining the magnetic interactions and establishing a correlation between the critical exponents and exchange integral responsible for ferromagnetic transition. The critical exponents near the PM-FM transition in the austenite phase of $\text{Ni}_{43}\text{Mn}_{46}\text{Sn}_8\text{X}_3$ ($\text{X} = \text{In}$ and Cr) Heusler alloys have been analysed within the framework of long range mean-field theory [45]. The recent results show deviation of critical exponents from the long range mean-field model, which is explained with two different behaviors that belonging to two different universality classes [46, 47]. Although, a close relationship between the critical behavior and magnetic exchange interaction has been perceived, a fundamental question about the universality class for PM-FM phase transition in these materials is still under debate, and hence need further investigation.

Here we investigate the MCE in the vicinity of PM-FM transition temperature of $\text{Co}_2\text{Cr}_{1-x}\text{Mn}_x\text{Al}$ alloys ($x = 0.25, 0.5, 0.75$). The powder x-ray diffraction patterns indicate all the samples to be single phase, and the $x = 0.75$ sample with L_{21} ordering. Our results mainly focus on the magnetic properties of these alloys and highlight the facts about the enhancement of magnetic moment, T_C and magnetic entropy change (ΔS_m) with Mn substitution for multi-stage magnetic refrigeration applications. These samples show relatively high T_C , which is very useful for technological applications and their structural and magnetic properties can be tuned easily/systematically. Therefore, understanding the critical behavior in $\text{Co}_2\text{Cr}_{1-x}\text{Mn}_x\text{Al}$ would provide the information about the nature of the magnetic phase transition and spin interaction in these systems. We have performed a detailed analysis and extracted the critical exponents for the $x = 0.75$ sample to understand the magnetocaloric properties. We found that the obtained parameters using modified Arrott plot (MAP) and Kouvel-Fisher (KF) method are very close to those expected for the mean field theory. The decay in the interaction distance sug-

gests for the existence of the long-range FM interactions in these samples. Also, we have discussed the field dependent relative cooling power (RCP) in relation to the critical behavior analysis for the $x = 0.75$ sample.

EXPERIMENTAL DETAILS

The polycrystalline samples of $\text{Co}_2\text{Cr}_{1-x}\text{Mn}_x\text{Al}$ ($x = 0.25, 0.5, 0.75$) have been prepared by melting the constituent elements using the arc furnace, from Centorr vacuum industries, USA. The proper stoichiometric amount of starting materials of Co, Cr, Mn, Al (from Alfa Aesar or Sigma Aldrich) with purity of $\geq 99.9\%$ were melted on water cooled Cu hearth in the flow of inert argon. Further, we flipped the solid ingot and the melting process was repeated 4–5 times for a better homogeneity. After melting the weight loss was found to be less than 0.8%. Then, the ingots were wrapped in the Mo sheet and sealed into the quartz tube under vacuum and annealed at 575 K for 10 days. The powder x-ray diffraction (XRD) measurements of $\text{Co}_2\text{Cr}_{1-x}\text{Mn}_x\text{Al}$ ($x = 0.25, 0.5, 0.75$) have been done with Cu $K\alpha$ ($\lambda = 1.5406 \text{ \AA}$) radiation at room temperature and the XRD patterns were refined by Rietveld method using FullProf package, where the background was fitted using linear interpolation between the data points. The magnetic measurements were performed using a vibrating sample magnetometer (VSM) option of a physical property measurement system (PPMS, Quantum Design, Inc.) at the core lab for quantum materials at Helmholtz-Zentrum Berlin.

RESULTS AND DISCUSSION

The X_2YZ Heusler alloys crystallize in the cubic structure (L_{21}) with space group $Fm\bar{3}m$. This unit cell consists of four interpenetrating bcc sublattices with X atoms positioned at $(1/4, 1/4, 1/4)$ and $(3/4, 3/4, 3/4)$, Y atom at $(0, 0, 0)$ and Z atom at $(1/2, 1/2, 1/2)$ sites [2]. We present the room temperature XRD patterns of $\text{Co}_2\text{Cr}_{1-x}\text{Mn}_x\text{Al}$ in Figs. 1(a–c) along with the Rietveld refinement using L_{21} structure and $Fm\bar{3}m$ (225) space group. We notice that (111) Bragg peak is not clearly visible in $x = 0.25$ and 0.5 samples. On the other hand, for the $x = 0.75$ sample we observed (111) Bragg peak at $2\theta \approx 26.7^\circ$, as shown in the inset of Fig. 1(c). In general, the presence of (111) and (200) Bragg peaks in XRD confirms the L_{21} type ordering in full Heusler alloys i.e., all the atoms are occupying their own positions. However, absence of only (111) Bragg peak indicates the B2 type atomic ordering in the system, which generally appears due to random occupation between Cr/Mn and Al atoms. The intensity ratio between (111) and (200) peaks can give idea about the degree of disorder present in the system. The refinement and measured XRD pat-

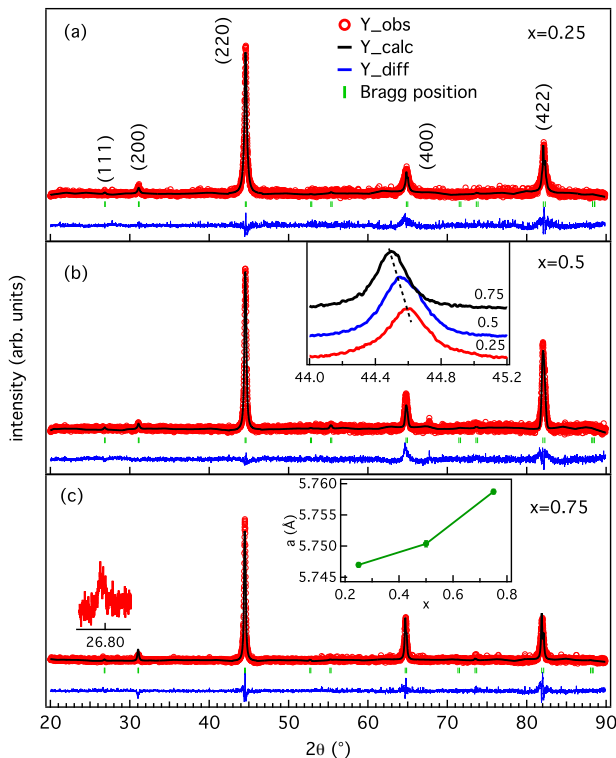


FIG. 1. The XRD patterns along with Rietveld refinement for the $x = 0.25$ (a), 0.5 (b), and 0.75 (c) samples. Insets in (b) and (c) show shift in 220 Bragg peak position and variation of lattice constant a with x , respectively, another inset in (c) is highlighting the presence of (111) Bragg peak at $\approx 26.7^\circ$.

terns show that Mn substitution at Cr site increases the degree of ordering [48] and confirm the $L2_1$ structure in the $x = 0.75$ sample. Moreover, we observed the shift in the (220) Bragg peak towards the lower 2θ value with increasing the x , as shown in the inset of Fig. 1(b) and consequently lattice constant a increases slightly with the Mn substitution (the x value), see the inset of Fig. 1(c). This increase in a is contrary to the expectation as the radius of Mn is smaller than Cr.

Figures 2(a-c) show the isothermal magnetization $M(H)$ data of $\text{Co}_2\text{Cr}_{1-x}\text{Mn}_x\text{Al}$ for the $x = 0.25, 0.5$ and 0.75 samples measured at 300 K. Interestingly, these samples exhibit a soft ferromagnetic behavior and the total magnetic moment calculated from isothermal magnetization at 300 K increases with the Mn substitution, as expected from the Slater-Pauling (SP) equation [4, 48] $M_t = (N_V - 24)$, where M_t and N_V are magnetic moment in Bohr magneton per formula unit ($\mu_B/f.u.$) and the number of valence electrons per formula unit, respectively. An increase in Mn concentration would imply an increased number of valence electrons in the sample (as Mn has one more valence electron than Cr); hence, the calculated magnetic moment according to the SP equation is expected to increase, as shown in the inset of Fig. 2(d). For comparison, we have plotted the magnetic

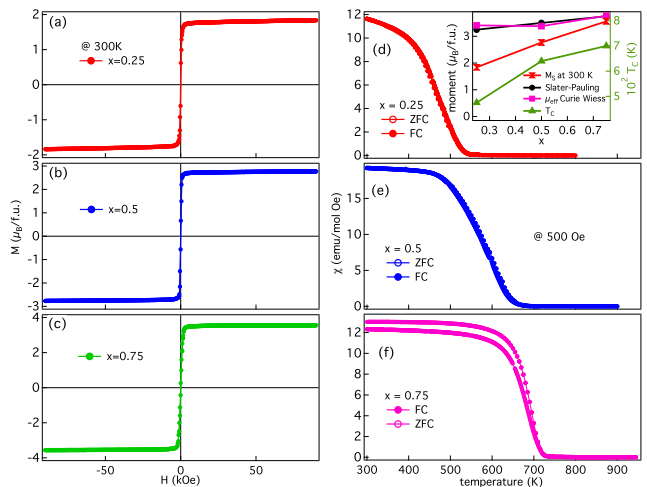


FIG. 2. (a-c) Isothermal magnetization M as a function of field H measured at 300 K and (d-f) Zero-field-cooled (ZFC) and field-cooled (FC) magnetic susceptibility χ with temperature measured at 500 Oe field for the $\text{Co}_2\text{Cr}_{1-x}\text{Mn}_x\text{Al}$ ($x = 0.25, 0.5, 0.75$) samples. Inset in (d) shows the variation of magnetic moment calculated from different methods (SP rule, saturation magnetization, Curie Weiss law) and T_C with x .

moment values (saturation magnetization, M_S) from the isothermal magnetic measurements in FM state at 300 K. We note that the experimental values show an increasing behavior as expected from the SP rule. However, the lower values as compare to the SP rule for the $x = 0.25$ and 0.5 samples might be due to the presence of atomic disorder, which is suggested to reduce the ferromagnetic ordering (moment) in these Heusler alloys [49, 50]. On the other hand, for the $x = 0.75$ sample, the M_S is almost same as calculated from the SP equation. This is also consistent with the fact that we observed (111) Bragg peak, which confirms $L2_1$ ordered state in the $x = 0.75$ sample. The thermomagnetic ZFC (zero field cooled) and FC (field cooled) curves have been shown in Figs. 2(d-f) for all the samples. The consistent decrease in magnetization with temperature and absence of thermal hysteresis indicate a second order PM to FM phase transition. The reported T_C of the parent sample Co_2CrAl is close to the room temperature (315 K) [17, 18]. It should be noted that the Mn substitution at the Cr site in Co_2CrAl strongly influences the Curie temperature (T_C) and μ_{eff} obtained from the Curie-Weiss law. As shown in the inset of Fig. 2(d), the T_C increases with the Mn concentration. This indicates that the substitution of Mn at Cr site increases the T_C from 315 K ($x = 0$ sample) to about 720 K for the $x = 0.75$ sample. Interestingly, the absence of thermal hysteresis in $M-T$ data [Figs. 2(d-f)] is the signature of SOPT in these samples (detailed analysis discussed later), which makes them a favorable candidate and motivate to investigate the magnetocaloric properties. The influence of Mn substitution on the T_C

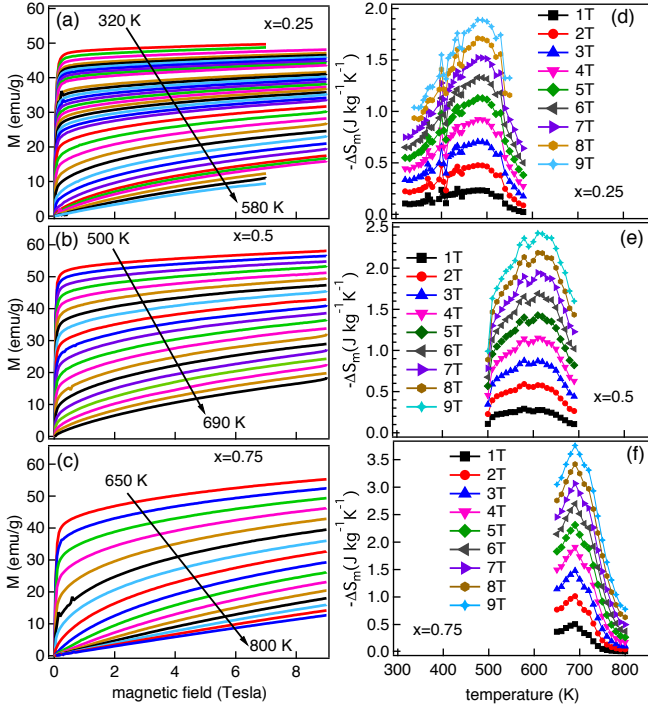


FIG. 3. Isothermal magnetization $M(H)$, change in magnetic entropy (ΔS_m) with temperature for the $\text{Co}_2\text{Cr}_{1-x}\text{Mn}_x\text{Al}$ (a, d) $x = 0.25$, (b, e) $x = 0.5$ and (c, f) $x = 0.75$ samples.

is beneficial for controlling the working temperatures for spintronic and magnetic refrigerant applications.

The isothermal magnetization data measured across the transition temperature (T_C) and presented in Figs. 3(a-c) are used to investigate the magnetocaloric effect (MCE) of $\text{Co}_2\text{Cr}_{1-x}\text{Mn}_x\text{Al}$ ($x = 0.25, 0.5, 0.75$). The change in magnetic entropy (ΔS_m) with temperature has been obtained at different magnetic fields from 1 to 9 Tesla using the following Maxwell's relation:

$$\Delta S_m = \int_0^H \left(\frac{\delta M(H, T)}{\delta T} \right)_H dH \quad (1)$$

Figs. 3(d-f) show the variation of entropy change (ΔS_m) with temperature across T_C upto 9 Tesla field strength for $\text{Co}_2\text{Cr}_{1-x}\text{Mn}_x\text{Al}$ ($x = 0.25, 0.5, 0.75$) samples. All the samples show a peak in ΔS_m around the transition temperature. We can clearly see the increase in maximum (ΔS_m^{max}) value with increase in the x (Mn concentration). Although, the peak value of ΔS_m is lower in SOPT materials as compared to FOPT materials, no hysteresis loss is observed in SOPT materials and hence their refrigeration capacity (RC) can be more useful, discussed in detail later. The calculated values of ΔS_m^{max} are 1.9 and 2.4 J/kg.K at 9 Tesla for the $x = 0.25$ and 0.5 samples, respectively. However, highest ΔS_m^{max} value was found for the $x = 0.75$ sample, which is 3.8 J/kg.K at 9 Tesla. We note that the highest value of ΔS_m^{max} for the $x = 0.75$ sample is relatively lower compare to

the other known SOPT materials like expensive Gd [27]. On the other hand, high value of ΔS_m^{max} can be found in transition metal based intermetallic alloys, for example Ni_2MnIn (6.3 J/kg.K at 5 Tesla) [51], Pt-doped Ni-Mn-Ga (7 J/kg.K at 5 Tesla) [52], $\text{MnFeP}_{0.45}\text{As}_{0.55}$ (18 J/kg.K at 5 Tesla) [31], etc. However, the increasing behavior of ΔS_m^{max} and broad temperature range is suitable for Ericsson-cycle magnetic refrigerant applications [53]. In this direction, it is important to note that understanding the magnetic properties and MCE makes Co_2 -based Heusler alloys useful for both spintronics and multi-stage magnetic refrigerators.

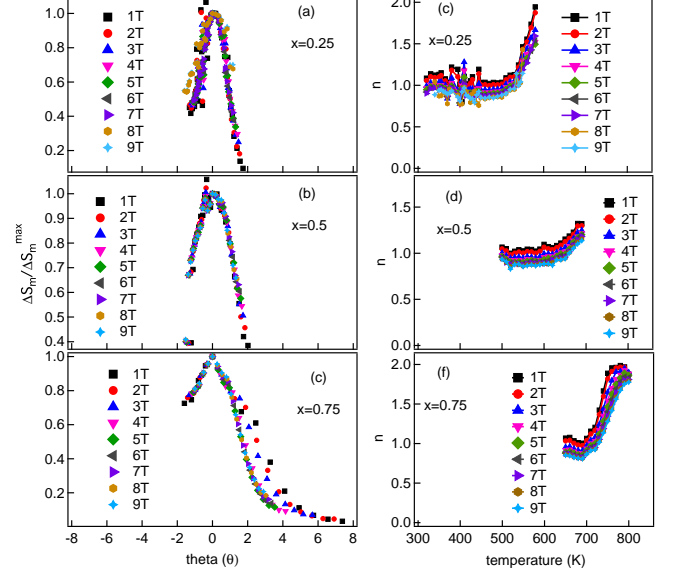


FIG. 4. (a-c) The scaled change in entropy with scaled temperature and (d-f) the variation of n with temperature obtained at different applied magnetic fields for the $\text{Co}_2\text{Cr}_{1-x}\text{Mn}_x\text{Al}$ ($x = 0.25, 0.5, 0.75$) samples.

Franco and Conde first proposed a method to check the nature of magnetic phase transition by the MCE. According to this method, for the second order magnetic phase transition (SOPT), all the entropy curves at different applied fields should collapse into a single curve after scaling [54]. In these curves the entropy has been normalized and temperature axis is scaled into θ , which is defined as [55]:

$$\theta = \begin{cases} -(T - T_{pk})/(T_{r1} - T_{pk}); & T \leq T_C \\ (T - T_{pk})/(T_{r2} - T_{pk}); & T > T_C \end{cases} \quad (2)$$

where T_{r1} and T_{r2} are the reference temperatures below and above the T_C , respectively, corresponding to certain f value and T_{pk} is the temperature corresponding to peak value of ΔS_m . In our case $f = \Delta S_m/\Delta S_m^{max} = 0.8$ has been chosen for all the samples. Figures. 4(a-c) show the variation of $\Delta S_m/\Delta S_m^{max}$ as a function of scaled temperature θ . As evident from Figs. 4(a-c), all

the curves at different applied fields upto 9 Tesla collapses into a single curve, which is the signature of SOPT in $\text{Co}_2\text{Cr}_{1-x}\text{Mn}_x\text{Al}$ ($x = 0.25, 0.5, 0.75$) samples.

Further analysis of the MCE in $\text{Co}_2\text{Cr}_{1-x}\text{Mn}_x\text{Al}$ samples, in the case of mean field model, gives a direction to check the dependency of ΔS_m with applied magnetic field. The ΔS_m has a power law dependency with the field as $|\Delta S_m| = a(H)^n$, where a is a constant and n is an exponent of magnetic entropy change that depends on the magnetic state of the material. From the entropy change curves, n at different applied fields across the transition temperature can be calculated as [56]:

$$n = \frac{d(\ln|\Delta S_m|)}{d(\ln H)} \quad (3)$$

The dependency of n on temperature have been thoroughly explored for SOPT materials in earlier reports [55]. For a small field, the value of n can not be considered due to multi domain state in the sample. The temperature and field dependent n is shown in Figs. 4(d-f), where at temperatures well below and above the T_C , the value of n found to be equal to 1 and 2, respectively. This means in this temperature range across the transition n changes from 1 to 2 i.e., $n = 1$ at fairly ferromagnetic region, attains its minimum value at T_C and $n = 2$ in the paramagnetic region as a consequence of Curie-Weiss law, unlike FOPT type materials where $n > 2$ [57]. This analysis confirms the nature of second order type magnetic transition in the present study and is also consistent with a recent interesting study by Law *et al.* [57].

The magnetization study shows the magnetic transition from PM to FM state, as also shown by the M as a function of H for selected temperatures near the phase transition, T_C . In general, we get more information about the PM-FM transition from Arrott plots, where M^2 vs H/M curves should have the parallel lines in high field region for the mean field model. The Arrott plot is the alternative method to get an idea about the nature of phase transition. According to Banerjee criterion positive and negative slope of straight line fit in Arrott plot is the signature of SOPT and FOPT nature, respectively [58]. From the Arrott plot and Banerjee criterion, we can conclude that $\text{Co}_2\text{Cr}_{1-x}\text{Mn}_x\text{Al}$ ($x = 0.75$) exhibits a second order phase transition. Moreover, the magnetization curves near PM-FM phase transition temperature should follow the Arrott-Noakes equation of state [59]:

$$\left(\frac{H}{M}\right)^{\frac{1}{\gamma}} = a \frac{(T - T_c)}{T} + bM^{\frac{1}{\beta}} \quad (4)$$

where a , b are constants. The β , γ and T_C are critical exponents and Curie temperature, respectively. This equation gives a set of parallel straight lines with correct combination of β , γ and T_C .

In order to understand the nature of magnetic phase transition near T_C , the nature of the ordering and the

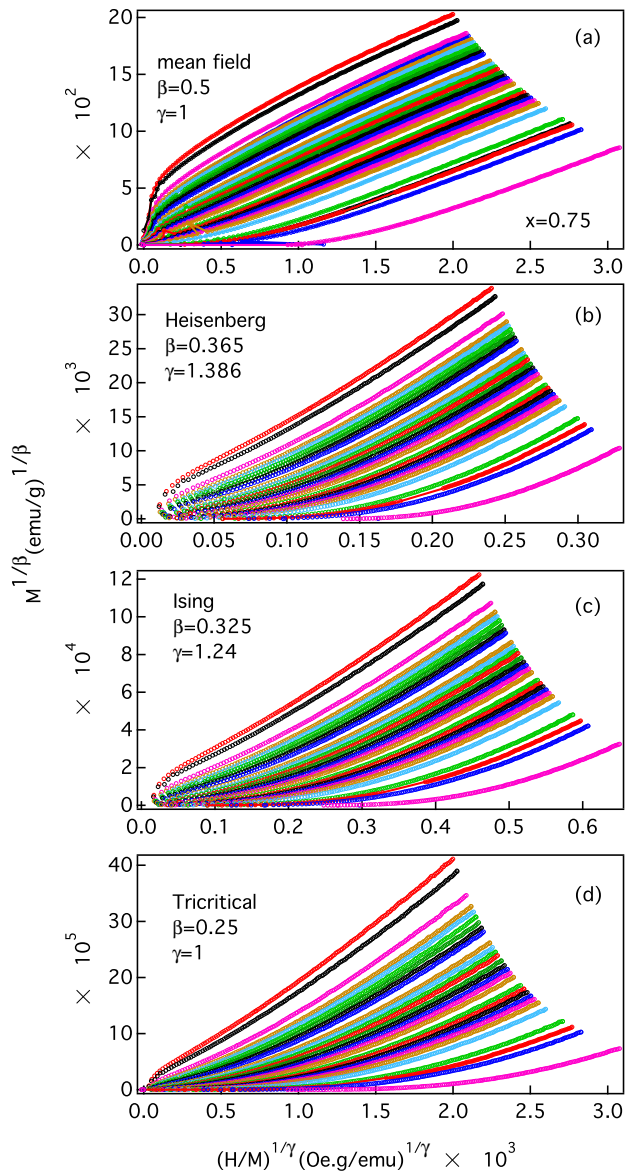


FIG. 5. Isotherms $M^{1/\beta}$ vs $(H/M)^{1/\gamma}$ using (a) mean field, (b) Heisenberg, (c) Ising and (d) Tricritical mean field models for the $x = 0.75$ sample.

MC behavior of $\text{Co}_2\text{Cr}_{1-x}\text{Mn}_x\text{Al}$, we have performed detailed analysis to extract the values of critical exponents (β , γ and δ) for the $x = 0.75$ sample. Here, the critical exponents β , γ and δ are correspond to the saturation magnetization $M_S(T)$, the inverse initial magnetic susceptibility χ_0^{-1} and the critical magnetization at T_C , respectively [59]. The critical exponents β and γ can be calculated using the following equations [60, 61]:

$$M_S(T) = M_0(-\epsilon)^\beta; \quad \epsilon < 0, T < T_c \quad (5)$$

$$\chi_0^{-1} = \frac{h_0}{M_0}(\epsilon)^\gamma; \quad \epsilon > 0, T > T_c \quad (6)$$

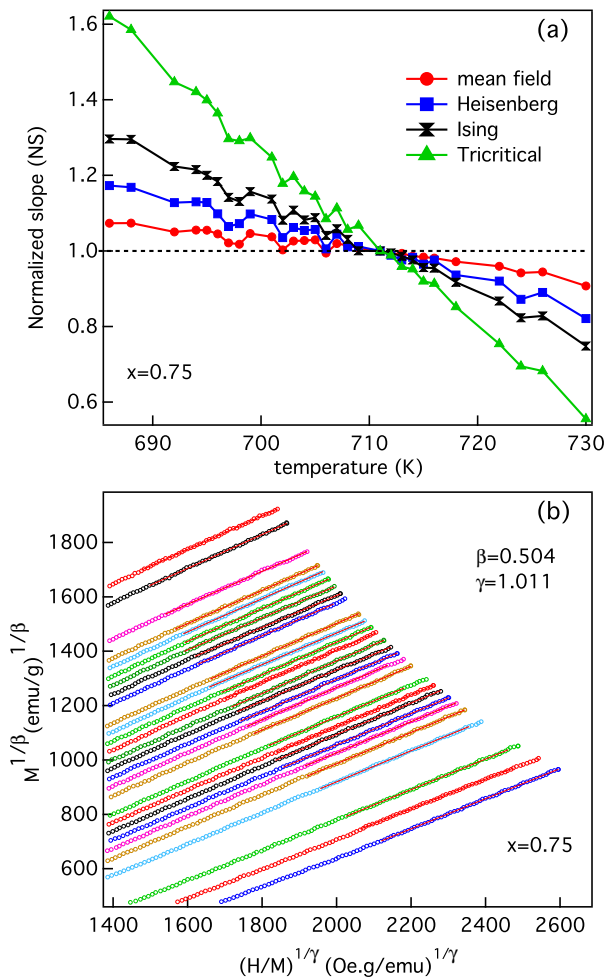


FIG. 6. (a) The temperature dependence of normalized slope (NS) of four different models and (b) the modified Arrott plot ($M^{1/\beta}$ vs $(H/M)^{1/\gamma}$) of isotherms for the $x = 0.75$ sample.

where $\epsilon = [(T - T_C)/T_C]$ and h_0/M_0 are the reduced temperature and the critical amplitude, respectively. More details about the physical meaning of these critical amplitudes can be found in refs. [61, 62].

As there can be different types of magnetic interactions corresponding to the spin-dimensionality d (discussed later) [63, 64], the Heisenberg model shows isotropic magnetic coupling, when $d = 3$, whereas $d = 1$ belongs to the Ising model and corresponds to an anisotropic magnetic interaction [64]. The tricritical model is applicable to the multiple phase system [65]. These four models have been considered for initial assumption of β and γ values i.e. mean field model ($\beta = 0.5$, $\gamma = 1$), Heisenberg model ($\beta = 0.365$, $\gamma = 1.386$), Ising model ($\beta = 0.325$, $\gamma = 1.24$) and tricritical model ($\beta = 0.25$, $\gamma = 1$). First we use these values of β and γ to construct modified Arrott plots [$M^{1/\beta}$ vs $(H/M)^{1/\gamma}$], which for all the four models are shown in Figs. 5(a–d) for the $x = 0.75$ sample. The best model can be decided by two criteria: (1) all the

lines in the high field region in $M^{1/\beta}$ vs $(H/M)^{1/\gamma}$ plot should be straight and (2) they should be parallel to each other. The plots of $M^{1/\beta}$ vs $(H/M)^{1/\gamma}$ should exhibit a set of straight lines parallel to each other with same slope $S(T)$ around T_C . The line which passes through origin will define the Curie temperature (T_C). Although, all the models have straight lines in high field region, the slope is not same near T_C . To further check the second criteria normalized slope (NS) has been calculated. The NS , expressed as $NS = S(T)/S(T_C)$, has been calculated at each temperature near T_C , where $S(T)$ is the slope of $M^{1/\beta}$ vs $(H/M)^{1/\gamma}$ at temperature T and $S(T_C)$ is the slope at T_C . For a best fit model, the value of NS should be almost equal to one.

Figure 6(a) shows the temperature variation of NS for the $x = 0.75$ sample fitted for modified Arrott plots. We find that the critical behavior of the $\text{Co}_2\text{Cr}_{0.25}\text{Mn}_{0.75}\text{Al}$ sample is described best by the mean field model. Note that initially we constructed a modified Arrott plot using equation 4 with a set of β and γ values according to the mean field model. Then the best values of β and γ were obtained by iteration method [66] using equations 5 and 6. The $M_S(T, 0)$ and $\chi_0^{-1}(T, 0)$ for zero field are estimated from the linear extrapolation of $M^{1/\beta}$ vs $H/M^{1/\gamma}$ lines in high field region to the positive intercept on $M^{1/\beta}$ (below T_c) and $H/M^{1/\gamma}$ (above T_C) axes, respectively and the fitting of the curves with equations 5 and 6 yields new β , γ and T_C . This process is iterated until we get the stable values of β and γ . After few iterations the modified Arrott plot with so obtained $\beta = 0.504$, $\gamma = 1.011$ for the $x = 0.75$ sample is shown in Fig. 6(b), which forms the set of parallel lines in high field region. However, the lines in the low field region are curved due to different domains magnetized in different directions. To further check the critical exponents, the intercept of $M^{1/\beta}$ and $(H/M)^{1/\gamma}$ from Fig. 6(b) gives M_S and χ_0^{-1} , respectively and fitting of M_S vs T and χ_0^{-1} using equations 5 and 6 gives the new set of critical exponents i.e. $\beta = 0.502$, $\gamma = 1.006$, as plotted in Fig. 7(a). The values of these critical exponents are quite close to the values obtained in Fig. 6(b).

Furthermore, we use Kouvel-Fisher method in order to validate the accuracy of these critical exponents determined from the modified Arrott plot, where the modified equations 5 to 6 are written below as per the Kouvel-Fisher method [60, 61]:

$$\frac{M_S(T)}{dM_S(T)/dT} = \frac{T - T_c}{\beta} \quad (7)$$

$$\frac{\chi_0^{-1}(T)}{d\chi_0^{-1}(T)/dT} = \frac{T - T_c}{\gamma} \quad (8)$$

$$\ln M(H, T_c) = \frac{\ln H}{\delta} \quad (9)$$

TABLE I. The critical exponents (α , β , γ and δ) determined from modified Arrott plot, Kouvel-Fisher method and critical isotherm for $\text{Co}_2\text{Cr}_{0.25}\text{Mn}_{0.75}\text{Al}$. The values of these parameters for Co_2CrAl (from [40]) and calculated from theoretically predicted universality classes have also been included for direct comparison.

Sample/Model	Reference(s)	Method(s)	α	β	γ	δ
Co_2CrAl	[40]	Modified Arrott plot		0.488 ± 0.003	1.144 ± 0.004	3.336 ± 0.005
		Kouvel-Fisher method		0.482 ± 0.013	1.148 ± 0.016	3.382 ± 0.020
		Critical isotherm				3.401 ± 0.004
$\text{Co}_2\text{Cr}_{0.25}\text{Mn}_{0.75}\text{Al}$	This work	Modified Arrott plot		0.503 ± 0.025	1.006 ± 0.050	3.004 ± 0.140
		Kouvel-Fisher method		0.507 ± 0.026	1.056 ± 0.055	3.083 ± 0.152
		Critical isotherm				2.903 ± 0.003
Mean field	[67, 68]	Theoretical	0	0.5	1.0	3.0
3D Heisenberg	[64, 67, 69]	Theoretical	-0.115	0.365	1.386	4.80
3D Ising	[64, 67, 69]	Theoretical	0.11	0.325	1.241	4.82
Tricritical mean field	[70]	Theoretical		0.25	1.0	5.0

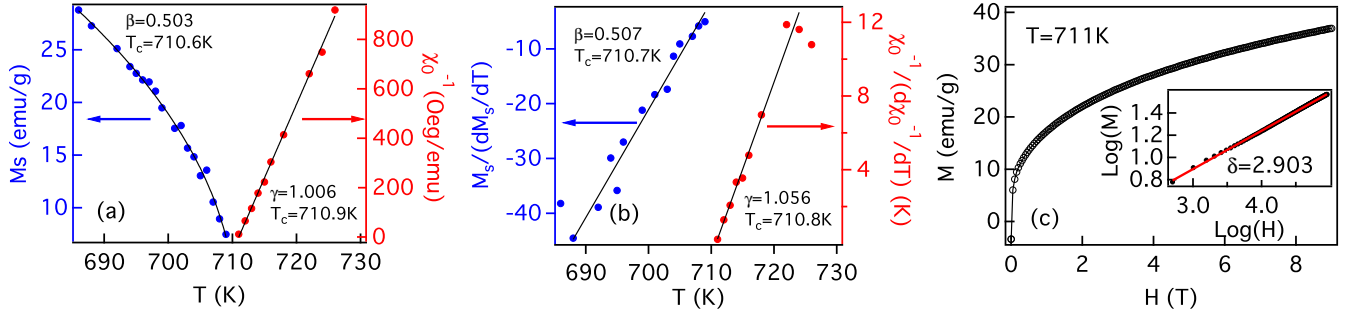


FIG. 7. (a) The plot of M_S (left axis) and χ_0^{-1} (right axis) as a function of temperature, (b) Kouvel-Fisher plot of M_S (left axis) and χ_0^{-1} (right axis) as a function of temperature, and (c) M vs H plot at 711 K for the $x = 0.75$ sample. The inset in (c) is the same plot in log-log scale with the linear fit (solid red line).

Here the critical exponents (β and γ) are obtained from the plots of $M_S (dM_S/dT)^{-1}$ vs T and $\chi_0^{-1} (d\chi_0^{-1}/dT)^{-1}$ vs T , as shown in Fig. 7(b). A linear fit to these two curves yields critical exponents where the values of $1/\beta$ and $1/\gamma$ are determined from the respective slope according to the equations 7 and 8, respectively, as shown in Fig. 7(b). Also, an intercept on x -axis for each curve corresponds to the T_C . In addition, according to the equation 9, the plot between $\ln(M)$ and $\ln(H)$ at T_C should be a straight line with slope of $1/\delta$. In the inset of Fig. 7(c), we show the straight line fit, which gives rise the value of $\delta = 2.903$. Moreover, we have utilized another method to check the reliability of δ value using Widom scaling relation $\gamma - \beta(\delta - 1) = 0$. The obtained critical exponents from Kouvel-Fisher method are very close to the values determined from Arrott-Noakes equation of state, as listed in Table I. The theoretically calculated parameters are also listed in Table I.

In the present case, the values of calculated critical exponents β and γ are close to the mean field model, which suggests for the presence of long range magnetic interactions in the system [67]. However, it is vital to

further confirm this inference. Therefore, it is important to check the scaling equation of state with these critical exponents [37, 71, 72]. The scaling equation of state which describes the relationship between $M(H, \epsilon)$, H and T_C can be expressed as:

$$M(H, \epsilon) = \epsilon^\beta f_{\pm} \left(\frac{H}{\epsilon^{\beta+\gamma}} \right) \quad (10)$$

where f_- and f_+ are regular analytical functions below and above T_C , respectively. The equation 10 states that for the proper combination of β , γ and T_C , the plot of scaled magnetization $m = |\epsilon|^{-\beta} M(H, \epsilon)$ as a function of scaled field $h = |\epsilon|^{-(\beta+\gamma)} H$ would generate the two distinct branches across the Curie temperature T_C . Using equation 10, the scaled m vs scaled h has been plotted in Fig. 8(a) with the above calculated critical exponents (β , γ) and T_C . It demonstrates that all the data have separated in two branches below and above T_C , where different symbols correspond to different temperatures. The inset in Fig. 8(a) is the same plot, but shown on a log-log scale. The reliability of the exponents and T_C has been further ensured with more rigorous analysis method by plotting m^2 vs h/m [Fig. 8(b)], where this plot falls

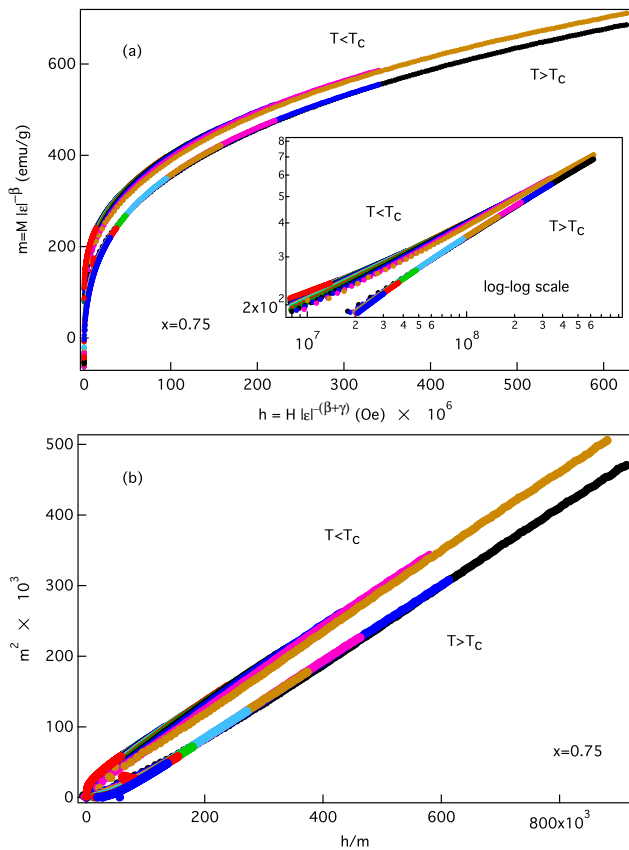


FIG. 8. (a) The renormalized magnetization (m) plotted (in left) as a function of renormalized field (h) and (b) the plot in form of m^2 vs h/m for the $x = 0.75$ sample. The different symbols correspond to different temperatures and the inset in (a) shows the log-log plot.

in two different branches across the T_C .

In the previous section we mentioned that the magnetic interactions in the studied samples are of extended type. Therefore, understanding the nature and range of spin interactions become an important part of this study. The extended type spin interaction is expressed in terms of exchange distance by $J(r)$, in which the long range exchange interaction decays as $J(r) \sim r^{-(D+\sigma)}$ and the short range exchange interaction decays as $J(r) \sim e^{-r/b}$, where r is the distance, D is the lattice dimensionality, σ is the range of interaction and b is special scaling factor [73]. The σ can be calculated by renormalization group approach using the following equation [63, 64]:

$$\gamma = 1 + \frac{4}{D} \frac{d+2}{d+8} \Delta\sigma + \frac{8(d+2)(d-4)}{D^2(d+8)^2} \Delta\sigma^2 \times \left[1 + \frac{2G(\frac{D}{2})(7d+20)}{(d-4)(d+8)} \right] \Delta\sigma^2 \quad (11)$$

where d is the spin dimensionality, $\Delta\sigma = \sigma - \frac{D}{2}$, $G(\frac{D}{2}) = 3 - \frac{1}{4}(\frac{D}{2})^2$. According to this equation for the experimental value of γ one can calculate the value of σ . Then

the obtained σ value can be used to calculate the other exponents using the expressions: $v = \gamma/\sigma$, $\alpha = 2 - vD$, $\beta = (2 - \alpha - \gamma)/2$ and $\delta = 1 + \gamma/\beta$, where v is the correlation length exponent. In the present study, for $d > 1$ and $D = 3$, the β and δ are close to our previous experimental results calculated by K-F method only for σ close to $3/2$, which is less than 2. For three-dimensional material ($D = 3$) mean field model ($\beta=0.5$, $\gamma=1$, $\delta=3.0$), the exchange interaction decays slower than power law of $J(r) \sim r^{-(3+\sigma)}$, which is only valid when $\sigma < 2$. It is known that $\sigma < 2$ corresponds to the long range spin interaction and $\sigma > 2$ indicates the short range interaction. This indicates that the exchange interaction, which belongs to the mean field model decays slower than $r^{-4.5}$. This analysis reveals the presence of long range spin interactions in the $x = 0.75$ sample.

As we discussed before, from the variation of n with temperature at various fields, we found the minimum value of $n \approx 0.80$ (field independent) below T_C , as shown in Figs. 4(d-f), which is close to the mean field model [74]. The values of n can also be obtained by the critical exponents β and γ at T_C i.e. by using $n(T_C) = 1 + (\beta - 1)/(\beta + \gamma)$. In fact, using this formula we estimate $n = 0.67$, as predicted by Oesterreicher and Parker for the mean field ($\beta = 0.5$, $\gamma = 1$, $\delta = 3$) model [74]. In order to understand the relation between the critical behavior and the MCE, we now move to the analysis to check the refrigerator capacity, which depends on the temperatures of the cold and hot sinks of the cooling system and the change in isothermal entropy in the whole temperature range of the cooling cycle i.e., indicates the quantity of heat transferred between the cold and hot ends in the magnetic refrigerant in one ideal thermodynamic cycle [75]. In this context, to find the suitability and efficiency of a magnetocaloric material, another parameter is defined as the relative cooling power (RCP), which is a property of the material, and its high value is desirable in cooling applications [76–79]. Here, we have investigated the RCP, which is the product of maximum entropy change and the temperature at full width half maximum (FWHM), as the equation below [76–79]:

$$RCP = |-\Delta S_m| \times \delta T_{FWHM} \quad (12)$$

where δT_{FWHM} has been calculated from the magnetic entropy curves [see Fig. 3(f)] by fitting with the Gaussian function. The magnetic entropy peak is relatively broad in our case, which gives rise to a large temperature span ($\delta T_{FWHM} \approx 75$ K at 9 Tesla). Notably, Engelbrecht *et al.* reported that a material with broad magnetic entropy peak is better than a material with a sharp peak for cooling applications, which suggests that a broad temperature distribution is more attractive for MCE [80]. The value of RCP extracted from the above equation monotonically increases with field and attains a maximum value of about 282 J/kg at 9 Tesla (Fig. 9), which is quite comparable with the other reported Co_2 -based

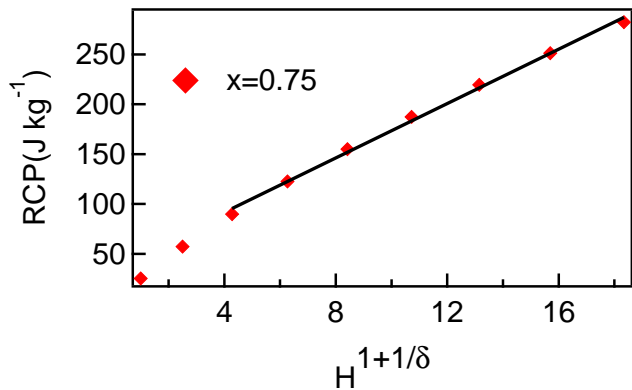


FIG. 9. The relative cooling power (RCP) with variation of $H^{1+\frac{1}{\delta}}$ for the $x = 0.75$ sample, where the solid black line is a simple linear fit.

Heusler alloys [40]. On the other hand, much higher value of RCP ≈ 400 J/kg at 5 Tesla has been reported for Gd [81]. Here the challenge is to find a rare earth free material and therefore, NiMnX alloys have been extensively studied for better performing MCE [82–85]. However, they mostly exhibit first order phase transition (FOPT), which causes a large thermal and magnetic hysteresis loss [82–85]. The present study makes the Co₂-based Heusler alloys a potential candidate for MCE even at a moderate RCP value where the transition temperature and maximum entropy change can be systematically controlled.

In addition, to emphasize the relation between the critical exponents and the magnetocaloric effect, the RCP can be expressed with the magnetic field power law. The field dependence of power law with exponent b is expressed as $\text{RCP} \propto H^b$ [86], where b is defined with the critical exponent δ as $b = 1 + \frac{1}{\delta}$. As listed in Table I, from the calculations of the critical behavior analysis, we find the value of $\delta = 3.083$ for Kouvel-Fisher method. Now taking into account this δ value, the plot of RCP vs field power ($H^{1+1/\delta}$) is shown in Fig. 9. A straight line fit with this power law matches well with the experimental data points, which establishes a correlation between MCE and critical behavior for the $x = 0.75$ sample. These experimental results and discussion suggest that these Heusler alloys exhibiting second order phase transition could be useful for high temperature cooling applications. Interesting to note that in a multi-stage magnetic refrigerator, the cooling from higher temperature is required in stage by stage manner [87]. These multi-stage refrigerators are very useful for industrial applications, where lower temperature in one stage acts as upper temperature for next stage [87, 88]. Therefore, these magnetic refrigerants with easily tunable magnetic moment and T_C can be useful at various operating temperatures. On the other hand, studies to find materials with considerable magnetocaloric effect near room temperature and investigation

of the critical behavior with additional probes including heat capacity that can measure direct adiabatic temperature change would be highly desirable [74].

CONCLUSIONS

In conclusion, we have performed a comprehensive analysis to study the MCE and the critical behavior of Co₂Cr_{1-x}Mn_xAl ($x = 0.25, 0.5, 0.75$) Heusler alloys. The PM-FM phase transition is found to be a second order phase transition. The scaled change in magnetic entropy with variation of scaled temperature at different fields collapse into single curve, which also confirms the second order nature of the transition. The determined critical exponents have values corresponding to universality classes of mean-field theory, and match well with the values calculated from modified Arrott plot, Kouvel-Fisher method and critical isotherm. On the other hand, the scaling theory separates the field dependent magnetization in two branches, below and above the T_C . The magnetic interactions in this alloy have been explained by the critical behavior and they follow the mean-field model with long range order magnetic interaction. The critical exponents estimated from the renormalization group approach are close to the obtained experimental values for $D = 3, d > 1$ that point towards the spin interaction of mean-field type with long range interaction and this interaction decays with distance r as $J(r) \sim r^{-4.5}$. The field dependent relative cooling power (RCP) has been studied and discussed to relate with the critical behavior analysis for the $x = 0.75$ sample. Interestingly, these high T_C materials can be used in multi-stage magnetic refrigerators where lower temperature in one stage acts as upper temperature for the next stage. Our study provides insight for making these Co₂ based Heusler alloys of practical use in both spintronic and magnetic cooling applications. However, the challenge remains to enhance magnetic entropy change (ΔS_m) and the relative cooling power by maintaining second order phase transition near room temperature.

ACKNOWLEDGMENTS

Priyanka Nehla acknowledges the MHRD, India for fellowship. We thank the physics department, IIT Delhi for providing XRD facility and support. This work was financially supported by the BRNS through DAE Young Scientist Research Award to RSD with project sanction No. 34/20/12/2015/BRNS.

* rsdhaka@physics.iitd.ac.in

- [1] F. Heusler, W. Starck, and E. Haupt, *Über magnetische Maganlegierung*, Verh. DPG **5**, 220 (1903).
- [2] T. Graf, C. Felser, and S. S. P. Parkin, Simple rules for the understanding of Heusler compounds, *Prog. Solid State Chem.* **39**, 1 (2011).
- [3] V. Alijani, J. Winterlik, G. H. Fecher, S. S. Naghavi, and C. Felser, Quaternary half-metallic Heusler ferromagnets for spintronics applications, *Phys. Rev. B* **83**, 184428 (2011).
- [4] I. Galanakis, Ph. Mavropoulos, and N. Papanikolaou, Slater-Pauling behavior and origin of the half-metallicity of the full-Heusler alloys, *Phys. Rev. B* **66**, 174429 (2002).
- [5] R. Kainuma, Y. Imano, W. Ito, Y. Sutou, H. Morito, S. Okamoto, O. Kitakami, K. Oikawa, A. Fujita, T. Kanomata, and K. Ishida, Magnetic-field-induced shape recovery by reverse phase transformation, *Nature* **439**, 957 (2006).
- [6] P. Devi, M. G. Zavareh, C. S. Mejjia, K. Hofmann, B. Albert, C. Felser, M. Nicklas, and S. Singh, Reversible adiabatic temperature change in the shape memory Heusler alloy $\text{Ni}_{2.2}\text{Mn}_{0.8}\text{Ga}$: An effect of structural compatibility, *Phys. Rev. Materials* **2**, 122401(R) (2018).
- [7] A. N. Vasil'ev, A. D. Bozhko, V. V. Khovailo, I. E. Dikshtein, V. G. Shavrov, V. D. Buchelnikov, M. Matsumoto, S. Suzuki, T. Takagi, and J. Tani, Structural and magnetic phase transitions in shape-memory alloys $\text{Ni}_{2+x}\text{Mn}_{1-x}\text{Ga}$, *Phys. Rev. B* **59**, 1113 (1999).
- [8] R. S. Dhaka, S. W. D'Souza, M. Maniraj, A. Chakrabarti, D. L. Schlagel, T. A. Lograsso, and S. R. Barman, Photoemission study of the (1 0 0) surface of Ni_2MnGa and Mn_2NiGa ferromagnetic shape memory alloys, *Surface Science* **603**, 1999 (2009).
- [9] Z. Wen, H. Sukegawa, S. Kasai, K. Inomata, and S. Mitani, Tunnel magnetoresistance and spin-transfer-torque switching in polycrystalline Co_2FeAl full-Heusler-alloy magnetic tunnel junctions on amorphous Si/SiO_2 substrates, *Phys. Rev. Applied* **2**, 024009 (2014).
- [10] S. A. Wolf, D. D. Awschalom, R. A. Buhrman, J. M. Daughton, S. von Molnár, M. L. Roukes, A. Y. Chtchelkanova, and D. M. Treger, Spintronics: a spin-based electronics vision for the future, *Science* **294**, 1488 (2001).
- [11] R. A. de Groot, F. M. Mueller, P. G. van Engen, and K. H. J. Buschow, New class of materials: half-metallic ferromagnets, *Phys. Rev. Lett.* **50**, 2024 (1983).
- [12] I. Galanakis and Ph. Mavropoulos, Spin-polarization and electronic properties of half-metallic Heusler alloys calculated from first principles, *J. Phys.: Condens. Matter* **19**, 315213 (2007).
- [13] T. Graf, S. S. P. Parkin, and C. Felser, Heusler compounds—a material class with exceptional properties, *IEEE Trans. Magn.* **47**, 367 (2011).
- [14] S. Wurmehl, G. H. Fecher, H. C. Kandpal, V. Ksenofontov, C. Felser, and H. Lin, Investigation of Co_2FeSi : The Heusler compound with highest Curie temperature and magnetic moment, *Appl. Phys. Lett.* **88**, 032503 (2006).
- [15] P. Nehla, C. Ulrich, R. S. Dhaka, Investigation of the structural, electronic, transport and magnetic properties of Co_2FeGa Heusler alloy nanoparticles, *J. Alloys Comp.* **776**, 379 (2019).
- [16] J. Kübler, G. H. Fecher, and C. Felser, Understanding the trend in the Curie temperatures of Co_2 -based Heusler compounds: Ab initio calculations, *Phys. Rev. B* **76**, 024414 (2007).
- [17] A. Husmann, and L. J. Singh, Temperature dependence of the anomalous Hall conductivity in the Heusler alloy Co_2CrAl , *Phys. Rev. B* **72**, 172417 (2006).
- [18] N. I. Kourov, A. V. Korolev, V. V. Marchenkov, A. V. Lukoyanov, and K. A. Belozerovala, Magnetic and electrical properties of the half-metallic ferromagnets Co_2CrAl , *Phys. Solid State* **55**, 977 (2013).
- [19] H. J. Elmers, G. H. Fecher, D. Valdaitsev, S. A. Nepijko, A. Gloskovskii, G. Jakob, G. Schonhense, S. Wurmehl, T. Block, C. Felser, P.-C. Hsu, W.-L. Tsai, and S. Cramm, Element-specific magnetic moments from core-absorption magnetic circular dichroism of the doped Heusler alloy $\text{Co}_2\text{Cr}_{0.6}\text{Fe}_{0.4}\text{Al}$, *Phys. Rev. B* **67**, 104412 (2003).
- [20] Y. J. Chen, D. Basiaga, J. R. O'Brien, and D. Heiman, Anomalous magnetic properties and Hall effect in ferromagnetic Co_2MnAl epilayers, *Appl. Phys. Lett.* **84**, 4301 (2004).
- [21] R. Y. Umetsu, K. Kobayashi, A. Fujita, R. Kainuma, and K. Ishida, Magnetic properties and stability of L_{21} and B_2 phases in the Co_2MnAl Heusler alloy, *J. Appl. Phys.* **103**, 07D718 (2008).
- [22] K. Ozdogan, E. Sasloglu, B. Aktas, and I. Galanakis, Doping and disorder in the Co_2MnAl and Co_2MnGa half-metallic Heusler alloys, *Phys. Rev. B* **74**, 172412 (2006).
- [23] J. Kubler, and C. Felser, Weyl points in the ferromagnetic Heusler compound Co_2MnAl , *Euro Physics Lett.*, **114**, 47005 (2016).
- [24] I. Galanakis, Appearance of half-metallicity in the quaternary Heusler alloys, *J. Phys.: Condens. Matter* **16**, 3089 (2004).
- [25] J. Kudrnovsky, V. Drchal, and I. Turek, Anomalous Hall effect in stoichiometric Heusler alloys with native disorder: A first-principles study, *Phys. Rev. B* **88**, 014422 (2013).
- [26] X. Zhang, H. Zhang, M. Qian, and L. Geng, Enhanced magnetocaloric effect in Ni-Mn-Sn-Co alloys with two successive magnetostuctural transformations, *Sci. Rep.* **8**, 8235 (2018).
- [27] S. Y. Dan'kov, A. M. Tishin, V. K. Pecharsky, and K. A. Gschneidner, Magnetic phase transitions and the magnetothermal properties of gadolinium, *Phys. Rev. B* **57**, 3478 (1998).
- [28] A. Planes, L. Mañosa, and M. Acet, Magnetocaloric effect and its relation to shape memory properties in ferromagnetic Heusler alloys, *J. Phys.: Condens. Matter* **21**, 233201 (2009).
- [29] M. Ovichi, H. Elbidweihy, E. D. Torre, L. H. Bennett, M. Ghahremani, F. Johnson, and M. Zou, Magnetocaloric effect in NiMnInSi Heusler alloys, *J. Appl. Phys.* **117**, 17D107 (2015).
- [30] V. V. Sokolovskiy, P. Entel, V. D. Buchelnikov, and M. E. Gruner, Achieving large magnetocaloric effects in Co- and Cr-substituted Heusler alloys: Predictions from first-principles and Monte Carlo studies, *Phys. Rev. B* **91**, 220409(R) (2015).
- [31] O. Tegus, E. Brück, K. H. J. Buschow, and F. R. de Boer, Transition-metal-based magnetic refrigerants for room-temperature applications, *Nature* **415**, 150 (2002).
- [32] V. Basso, C. P. Sasso, K. P. Skokov, O. Gutfleisch, and V. V. Khovaylo, Hysteresis and magnetocaloric effect at the magnetostuctural phase transition of Ni-Mn-Ga and Ni-Mn-Co-Sn Heusler alloys, *Phys. Rev. B* **85**, 014430 (2012).

- [33] T. Krenke, E. Duman, M. Acet, E. F. Wassermann, X. Moya, L. Maosa, and A. Planes, Inverse magnetocaloric effect in ferromagnetic Ni-Mn-Sn alloys, *Nature Materials* **4**, 450 (2005).
- [34] R. Sahoo, A. K. Nayak, K. G. Suresh, and A. K. Nigam, Effect of Si and Ga substitutions on the magnetocaloric properties of NiCoMnSb quaternary Heusler alloys, *J. Appl. Phys.* **109**, 07A921 (2011).
- [35] A. Fujita, S. Fujieda, Y. Hasegawa, and K. Fukamichi, Itinerant-electron metamagnetic transition and large magnetocaloric effects in $\text{La}(\text{Fe}_x\text{Si}_{1-x})_{13}$ compounds and their hydrides, *Phys. Rev. B* **67**, 104416 (2003).
- [36] H. Wada, and Y. Tanabe, Giant magnetocaloric effect of $\text{MnAs}_{1-x}\text{Sb}_x$, *Appl. Phys. Lett.* **79**, 3302 (2001).
- [37] M. Halder, S. M. Yusuf, and A. K. Nigam, Magnetocaloric effect and its implementation in critical behavior study of $\text{Mn}_4\text{FeGe}_{3-x}\text{Si}_x$ intermetallic compounds, *J. Appl. Phys.* **110**, 113915 (2011).
- [38] V. K. Pecharsky, and K. A. Gschneidner, Giant Magnetocaloric Effect in $\text{Gd}_5(\text{Si}_2\text{Ge}_2)$, *Phys. Rev. Lett.* **78**, 4494 (1997).
- [39] M. D. Kuz'min, Factors limiting the operation frequency of magnetic refrigerators, *Appl. Phys. Lett.* **90**, 251916 (2007).
- [40] J. Panda, S. N. Saha, and T. K. Nath, Critical behavior and magnetocaloric effect in $\text{Co}_{50-x}\text{Ni}_x\text{Cr}_{25}\text{Al}_{25}$ ($x = 0$ and 5) full Heusler alloy system, *J. Alloys Comp.* **644**, 930 (2015).
- [41] B. M. Wang, L. Wang, Y. Liu, and B. C. Zhao, A second-order ferromagnetic transition in the martensitic state of $\text{Ni}_{49.5}\text{Mn}_{32.5}\text{Cu}_4\text{Sn}_{14}$: A critical behavior study, *J. Appl. Phys.* **105**, 023913 (2009).
- [42] K. Ghosh, C. J. Lobb, R. L. Greene, S. G. Karabashiev, D. A. Shulyatev, A. A. Arsenov, and Y. Mukovskii, Critical phenomena in the double-exchange ferromagnet $\text{La}_{0.7}\text{Sr}_{0.3}\text{MnO}_3$, *Phys. Rev. Lett.* **81**, 4740 (1998).
- [43] A. J. Millis, P. B. Littlewood, and B. I. Shraiman, Double exchange alone does not explain the resistivity of $\text{La}_{1-x}\text{Sr}_x\text{MnO}_3$, *Phys. Rev. Lett.* **74**, 5144 (1995).
- [44] S. Mori, C. H. Chen, and S. W. Cheong, Paired and Unpaired Charge Stripes in the Ferromagnetic Phase of $\text{La}_{0.5}\text{Ca}_{0.5}\text{MnO}_3$, *Phys. Rev. Lett.* **81**, 3972 (1998).
- [45] W. Z. Nan, T. D. Thanh, G. Namc, T. S. You, H.G. Piao, L. Q. Pan, and S. C. Yu, Critical behavior near the ferromagnetic-paramagnetic transformation in the austenite phase of $\text{Ni}_{43}\text{Mn}_{46}\text{Sn}_8\text{X}_3$ ($X = \text{In}$ and Cr) Heusler alloys, *J. Magn. Magn. Mater.* **443**, 171 (2018).
- [46] P. Zhang, T. L. Phan, N. H. Duc, N. H. Dan, and S. C. Yu, Magnetocaloric and critical behaviors of $\text{Ni}_{0.5}\text{Mn}_{0.5-x}\text{Sn}_x$ Heusler alloys, *IEEE Trans. Magn.* **48**, 3753 (2012).
- [47] G. R. Raji, B. Uthaman, S. Thomas, K. G. Suresh, and M. R. Varma, Magnetocaloric properties, exchange bias, and critical behavior of Ge substituted $\text{Ni}_{50}\text{Mn}_{36}\text{Sn}_{14}$ Heusler alloys, *J. Appl. Phys.* **117**, 103908 (2015).
- [48] B. A. Alhaj, and B. Hamad, Ab-initio calculations of the electronic and magnetic structures of $\text{Co}_2\text{Cr}_{1-x}\text{Mn}_x\text{Al}$ alloys, *J. Appl. Phys.* **112**, 123904 (2012).
- [49] Y. V. Kudryavtsev, V. N. Uvarov, V. A. Oksenenko, Y. P. Lee, J. B. Kim, Y. H. Hyun, K. W. Kim, J. Y. Rhee, and J. Dubowik, Effect of disorder on various physical properties of Co_2CrAl Heusler alloy films: Experiment and theory, *Phys. Rev. B* **77**, 195104 (2008).
- [50] Y. Miura, K. Nagao, and M. Shirai, Atomic disorder effects on half-metallicity of the full-Heusler alloys $\text{Co}_2(\text{Cr}_{1-x}\text{Fe}_x)\text{Al}$: A first-principles study, *Phys. Rev. B.* **69**, 144413 (2004).
- [51] S. Singh, L. Caron, S. W. D'Souza, T. Fichtner, G. Porcari, S. Fabbrici, C. Shekhar, S. Chadov, M. Solzi, and C. Felser, Large magnetization and reversible magnetocaloric effect at the second-order magnetic transition in Heusler materials, *Adv. Mater.* **28**, 3321 (2016).
- [52] S. Singh, S. W. D'Souza, K. Mukherjee, P. Kushwaha, S. R. Barman, S. Agarwal, P. K. Mukhopadhyay, A. Chakrabarti, and E. V. Sampathkumaran, Magnetic properties and magnetocaloric effect in Pt doped Ni-Mn-Ga, *Appl. Phys. Lett.* **104**, 231909 (2014).
- [53] H. Takeya, V. V. Pecharsky, K. A. Gschneidner, and J. Moorman, New type of magnetocaloric effect: implications on low-temperature magnetic refrigeration using an Ericsson cycle, *Appl. Phys. Lett.* **64**, 2739 (1994).
- [54] C. M. Bonilla, J. H.-Albillos, F. Bartolomé, L. M. García, M. P.-Borderías, and V. Franco, Universal behavior for magnetic entropy change in magnetocaloric materials: An analysis on the nature of phase transitions, *Phys. Rev. B* **81**, 224424 (2010).
- [55] V. Franco, A. Conde, J. M. R.-Enrique, and J. S. Blazquez, A universal curve for the magnetocaloric effect: an analysis based on scaling relations, *J. Phys.: Condens. Matter* **20**, 285207 (2008).
- [56] V. Franco, R. Caballero-Flores, A. Conde, Q. Y. Dong, and H. W. Zhang, The influence of a minority magnetic phase on the field dependence of the magnetocaloric effect, *J. Magn. Magn. Mater.* **321**, 1115 (2009).
- [57] J. Y. Law, V. Franco, L. M. Moreno-Ramrez, A. Conde, D. Y. Karpenkov, I. Radulov, K. P. Skokov, and O. Gutfleisch, A quantitative criterion for determining the order of magnetic phase transitions using the magnetocaloric effect, *Nature Com.* **9**, 2680 (2018).
- [58] B. K. Banerjee, On a generalised approach to first and second order magnetic transitions, *Phys. Lett.* **12**, 16 (1964).
- [59] A. Arrott, and J. E. Noakes, Approximate equation of state for Nickel near its critical temperature, *Phys. Rev. Lett.* **19**, 786 (1967).
- [60] J. S. Kouvel, and M. E. Fisher, Detailed magnetic behavior of nickel near its Curie point, *Phys. Rev.* **136**, 1626 (1964).
- [61] M. E. Fisher, The theory of equilibrium critical phenomena, *Rep. Prog. Phys.* **30**, 615 (1967).
- [62] V. Siruguri, and S. N. Kaul, Detailed ferromagnetic resonance study of amorphous Fe-rich $\text{Fe}_{90-x}\text{Co}_x\text{Zr}_{10}$ alloys. II: critical behaviour and uniaxial anisotropy, *J. Phys.: Condens. Matter* **8**, 4567 (1996).
- [63] M. E. Fisher, S.-K. Ma, and B. G. Nickel, Critical exponents for long-range interactions, *Phys. Rev. Lett.* **29**, 917 (1972).
- [64] M. E. Fisher, The renormalization group in the theory of critical behavior, *Rev. Mod. Phys.* **46**, 597 (1974).
- [65] K. Huang, *Statistical Mechanics*, 2nd ed. (Wiley, New York, 1987).
- [66] L. Zhang, B. S.Wang, Y. P. Sun, P. Tong, J. Y. Fan, C. J. Zhang, L. Pi, and Y. H. Zhang, Critical behavior in the antiperovskite ferromagnet AlCMn_3 , *Phys. Rev. B* **85**, 104419 (2012).
- [67] S. N. Kaul, Static critical phenomena in ferromagnetics with quenched disorder, *J. Magn. Magn. Mater.* **53**, 5

- (1985).
- [68] H. E. Stanley, Introduction to phase transitions and critical phenomena, Oxford University Press, New York, 1971.
- [69] J. C. Le Guillou and J. Zinn-Justin, Critical exponents from field theory, *Phys. Rev. B* **21**, 3976 (1980).
- [70] D. Kim, B. Revaz, B. L. Zink, F. Hellman, J. J. Rhyne, J. F. Mitchell, Tricritical Point and the Doping Dependence of the Order of the Ferromagnetic Phase Transition of $\text{La}_{1-x}\text{Ca}_x\text{MnO}_3$, *Phys. Rev. Lett.* **89**, 227202 (2002).
- [71] A. K. Pramanik, and A. Banerjee, Critical behavior at paramagnetic to ferromagnetic phase transition in $\text{Pr}_{0.5}\text{Sr}_{0.5}\text{MnO}_3$: A bulk magnetization study, *Phys. Rev. B* **79**, 214426 (2009).
- [72] W. Yan, X. Zhang, Q. Shi, X. Yu, Z. Zhang, Q. Wang, S. Li, and H. Lei, Critical behavior of half-metallic ferromagnet $\text{Co}_3\text{Sn}_2\text{S}_2$, *Solid State Commun.* **281**, 57 (2018).
- [73] S. F. Fischer, S. N. Kaul, and H. Kronmüller, Critical magnetic properties of disordered polycrystalline $\text{Cr}_{75}\text{Fe}_{25}$ and $\text{Cr}_{70}\text{Fe}_{30}$ alloys, *Phys. Rev. B* **65**, 064443 (2002).
- [74] H. Oesterreicher, and F. T. Parker, Magnetic cooling near Curie temperatures above 300 K, *J. Appl. Phys.* **55**, 4334 (1984).
- [75] V. K. Pecharsky, and K. A. Gschneidner Jr., Some common misconceptions concerning magnetic refrigerant materials, *J. Appl. Phys.* **90**, 4614 (2001).
- [76] K. A. Gschneidner Jr., and V. K. Pecharsky, Magnetocaloric Materials, *Annu. Rev. Mater. Sci.* **30**, 387 (2000).
- [77] K. A. Gschneidner Jr., V. K. Pecharsky, and A. O. Tsokol, Recent developments in magnetocaloric materials, *Rep. Prog. Phys.* **68**, 1479 (2005).
- [78] M. H. Phan, and S. C. Yu, Review of the magnetocaloric effect in manganite materials, *J. Magn. Magn. Mater.* **308**, 325 (2007).
- [79] V. Markovich, A. Wisniewski, and H. Szymczak, in *Handbook of Magnetic Materials*, edited by K. H. J. Buschow (Elsevier, Amsterdam, 2014), volume 22, chapter 1, page 21, ISBN: 978-0-444-63291-3.
- [80] K. Engelbrecht, and C. R. H. Bahl, Evaluating the effect of magnetocaloric properties on magnetic refrigeration performance, *J. Appl. Phys.* **108**, 123918 (2010).
- [81] S. P. Mathew, and S. N. Kaula, Tuning magnetocaloric effect with nanocrystallite size, *Appl. Phys. Lett.* **98**, 172505 (2011).
- [82] F. X. Hu, B. G. Shen, and J. R. Sun, Magnetic entropy change in $\text{Ni}_{51.5}\text{Mn}_{22.7}\text{Ga}_{25.8}$ alloy, *Appl. Phys. Lett.* **76**, 3460 (2000).
- [83] M. G. Zavareh, C. S. Mejía, A. K. Nayak, Y. Skourski, J. Wosnitza, C. Felser, and M. Nicklas, Direct measurements of the magnetocaloric effect in pulsed magnetic fields: the example of the Heusler alloy $\text{Ni}_{50}\text{Mn}_{35}\text{In}_{15}$, *Appl. Phys. Lett.* **106**, 071904 (2015).
- [84] Z. Li, K. Xu, Y. Zhang, C. Tao, D. Zheng, and C. Jing, Two successive magneto-structural transformations and their relation to enhanced magnetocaloric effect for $\text{N}_{55.8}\text{Mn}_{18.1}\text{Ga}_{26.1}$ Heusler alloy, *Sci Rep.* **5**, 15143 (2015).
- [85] J.-H. Chen, N. M. Bruno, Z. Ning, W. A. Shelton, I. Karaman, Y. Huang, J. Li, J. H. Ross Jr., Relative cooling power enhancement by tuning magneto-structural stability in Ni-Mn-In Heusler alloys, *J. Alloys Compd.* **744**, 785 (2018).
- [86] M. Oumezzine, O. Pena, S. Kallel, and M. Oumezzine, Crossover of the magnetocaloric effect and its importance on the determination of the critical behaviour in the $\text{La}_{0.67}\text{Ba}_{0.33}\text{Mn}_{0.9}\text{Cr}_{0.1}\text{O}_3$ perovskite manganite, *J. Alloys Compd.* **539**, 116 (2012).
- [87] A. Kitanovski, and P. W. Egolf, Innovative ideas for future research on magnetocaloric technologies, *Int. J. Refrig.* **33**, 449 (2010).
- [88] V. Franco, J. S. Blázquez, J. J. Ipus, J. Y. Law, L. M. Moreno-Ramírez, and A. Conde, Magnetocaloric effect: From materials research to refrigeration devices, *Progress in Materials Science* **93**, 112 (2018).